Bioactive Materials 6 (2021) 3025–3035

Contents lists available at ScienceDirect

Bioactive Materials

journal homepage: www.sciencedirect.com/journal/bioactive-materials

Efficient drug delivery and anticancer effect of micelles based on vitamin E succinate and chitosan derivatives

Xiaotong Chen [a,1], Junxiang Gu [a,1], Le Sun [a], Wenya Li [a], Lili Guo [a], Zhiyang Gu [a], Litong Wang [a], Yan Zhang [a], Wangwang Zhang [a], Baoqin Han [a,b], Jing Chang [a,b,*]

[a] College of Marine Life Science, Ocean University of China, Qingdao, 266003, PR China
[b] Laboratory for Marine Drugs and Bioproducts, Pilot National Laboratory for Marine Science and Technology (Qingdao), Qingdao, 266235, PR China

ARTICLE INFO

Keywords:
Vitamin E succinate
Chitosan
Multi-drug resistance
Drug delivery
Nanocarrier

ABSTRACT

Nanocarriers have emerged as a promising cancer drug delivery strategy. Multi-drug resistance caused by overexpression of multiple-drug excretion transporters in tumor cells is the major obstacle to successful chemotherapy. Vitamin E derivatives have many essential functions for drug delivery applications, such as biological components that are hydrophobic, stable, water-soluble enhancing compounds, and anticancer activity. In addition, vitamin E derivatives are also effective mitocan which can overcome multi-drug resistance by binding to P glycoproteins. Here, we developed a carboxymethyl chitosan/vitamin E succinate nano-micellar system (*O*-CMCTS-VES). The synthesized polymers were characterized by Fourier Transform IR, and ^{1}H NMR spectra. The mean sizes of *O*-CMCTS-VES and DOX-loaded nanoparticles were around 177 nm and 208 nm. The drug loading contents were 6.1%, 13.0% and 10.6% with the weight ratio of DOX to *O*-CMCTS-VES corresponding 1:10, 2:10 and 3:10, and the corresponding EEs were 64.3%, 74.5% and 39.7%. Cytotoxicity test, hemolysis test and histocompatibility test showed that it had good biocompatibility *in vitro* and *in vivo*. Drug release experiments implied good pH sensitivity and sustained-release effect. The DOX/*O*-CMCTS-VES nanoparticles can be efficiently taken up by HepG2 cancer cells and the tumor inhibition rate is up to 62.57%. In the *in vivo* study by using H22 cells implanted Balb/C mice, DOX/*O*-CMCTS-VES reduced the tumor volume and weight efficiently with a TIR of 35.58%. The newly developed polymeric micelles could successfully be utilized as a nanocarrier system for hydrophobic chemotherapeutic agents for the treatment of solid tumors.

1. Introduction

The morbidity and mortality of malignant tumor are increasing year by year, and it ranks the first among all kinds of causes of death, seriously endangering the health of human beings. It is estimated that there may be 26.4 million newly diagnosed cancer cases worldwide by 2030, and approximately 17 million people may die from malignant tumors.

ATP production is mainly dependent on the oxidative phosphorylation pathway of mitochondria in normal cells, which is only dependent on glycolysis in the case of hypoxia. In contrast, about 50% of ATP in tumor cells is synthesized through glycolysis, and even in aerobic conditions, tumor cells prefer to use the glycolysis pathway to provide energy and produce lactic acid [1,2]. This process is known as the Warburg effect [3], which is also an important indicator of cancer. Mitochondria are the major sites of tumor cell metabolism, which are the energy supply factories of cell life activities and the organelles that control programmed cell death. Compared with normal mitochondria, mitochondria of tumor cells have more active metabolism, which can regulate intracellular ROS and ATP levels, signal transduction and apoptosis. Cancer cells expend more energy to maintain a high rate of cell division, which means they need more mitochondria than normal cells. In addition, mitochondria in cancer cells are more sensitive to mitocans, such as drugs that have therapeutic effects on mitochondria [4]. Therefore, mitochondria have become important targets of tumor metabolism therapy, and targeting mitochondria has attracted more and more attention in tumor therapy [5].

Vitamin E succinate (VES) is a well-known vitamin E derivative consisting of three domains [6], including hydrophobic domain, signal

Peer review under responsibility of KeAi Communications Co., Ltd.
* Corresponding author. College of Marine Life Science, Ocean University of China, Qingdao, 266003, PR China.
E-mail address: changjing@ouc.edu.cn (J. Chang).
[1] These two authors contributed equally to this work.

https://doi.org/10.1016/j.bioactmat.2021.02.028
Received 10 December 2020; Received in revised form 9 February 2021; Accepted 21 February 2021
Available online 9 March 2021

domain and functional domain [7]. Mitocan is a well-known anti-cancer compound that acts on mitochondria [8]. It can stimulate the production of reactive oxygen species by interacting with the coenzyme Q binding site of mitochondrial respiratory chain complex II [9], and meanwhile reduce mitochondrial membrane potential (MMP) and induce cell apoptosis [10]. VES also leads to the release of cytochrome C into the cytoplasm by destroying the stability of lysosomal membrane, further activating the caspase cascade and activating various caspases [9,11]. VES produces apoptosis in more than 50 types of cancer cell lines, including lung cancer, breast cancer, colon cancer, lymphoma, melanoma, etc. VES has been shown to be highly selective to cancer cells and very limited or no toxicity to normal cells [6,12]. Another important advantage of using VES in nanodrugs is that it acts as an inhibitor of the drug efflux transporter p-glycoprotein (P-GP), which can make multidrug resistant (MDR) tumors sensitive to a variety of anticancer drugs [13], including curcumin, doxorubicin, paclitaxel, and vincristine. However, the main drawback that prevents VES from being widely used in clinical treatment is its hydrophobicity [6]. In most studies of the anticancer effects of VES *in vitro* and *in vivo*, organic solvents including dimethyl sulfoxide (DMSO) and ethanol lead to unavoidable side effects. Therefore, it is necessary to develop a new approach for VES application to overcome its side effects.

Using the hydrophobicity of VES as hydrophobic block to construct amphiphilic self-assembled micelles is a very valuable application method. Due to their special sizes, polymer micelles could realize the advantages of passive targeting tumor through enhanced permeability and retention (EPR) effect [14]. Moreover, the micelles could avoid the traditional adverse side effects of chemotherapy, avoid fast kidney removal and extend the time of drug circulation, which could achieve sustained drug release behavior and improve the bioavailability and stability [15,16].

Amphiphilic polymers can be constructed by hydrophobic modification of hydrophilic polymers, thus self-assembled polymer micelle structure can be easily formed [17]. The physical stability of micelles can be adjusted by the polymer composition, hydrophobic length and block length ratio [18]. Common hydrophilic natural polymers include polysaccharides and proteins, among which chitosan has been widely used in pharmaceutical industry due to its non-toxic, biodegradable and good biocompatibility.

Chitosan is a natural cationic alkaline polysaccharide, which has been widely used in medicine, food, chemical and biotechnology field [19]. However, its biomedical application was restricted due to its poor water solubility, and it is difficult to be absorbed by the human body [20,21]. Carboxymethyl chitosan is the most important water-soluble derivative of chitosan. Compared to chitosan, carboxymethyl chitosan retains the excellent properties of chitosan and shows better water solubility [22]. The amphiphilic derivatives prepared by the hydrophobicity modification of carboxymethyl chitosan have been demonstrated by many researchers as potential carriers for loading hydrophobic drugs [23–25]. As shown in Scheme 1., motivated by the above-mentioned rationales, we first synthesized a novel amphiphilic polymer – carboxymethyl chitosan - α -Vitamin E Succinate (*O*-CMCTS-VES), which was anticipated to combine the advantages of both *O*-CMCTS and VES. The *O*-CMCTS-VES copolymers could form a nanoparticle structure by self-assembly action for targeted and intracellular transportation of Doxorubicin (DOX). The physiological characteristics and the antitumor efficacy of the DOX-loaded NPs were systematically evaluated, and the result showed high tumor inhibition rate both *in vitro* and *in vivo*. The results could provide a promising new carrier for drug delivery, which could be helpful for the treatment of cancer through chemotherapy method.

2. Materials and methods

2.1. Materials

Carboxymethyl chitosan (degree of deacetylation = 79.8%, degree of carboxymethyl substitution = 51.2%) was purchased from Qingdao Biotemed Biomaterial Co., Ltd (Qingdao, China). Vitamin E succinate (D-α-tocopherol succinate) and Fluorescein Isothiocyanate (FITC) were purchased from Sigma-Aldrich chemicals Pvt. Ltd. 1-ethyl-3-[3-(dimethylamino) propyl] carbodiimide (EDC·HCl) and N-Hydroxy succinimide (NHS) were purchased from solarbio science & technology co. Ltd (Beijing, China). Doxorubicin hydrochloride (DOX·HCl) was obtained

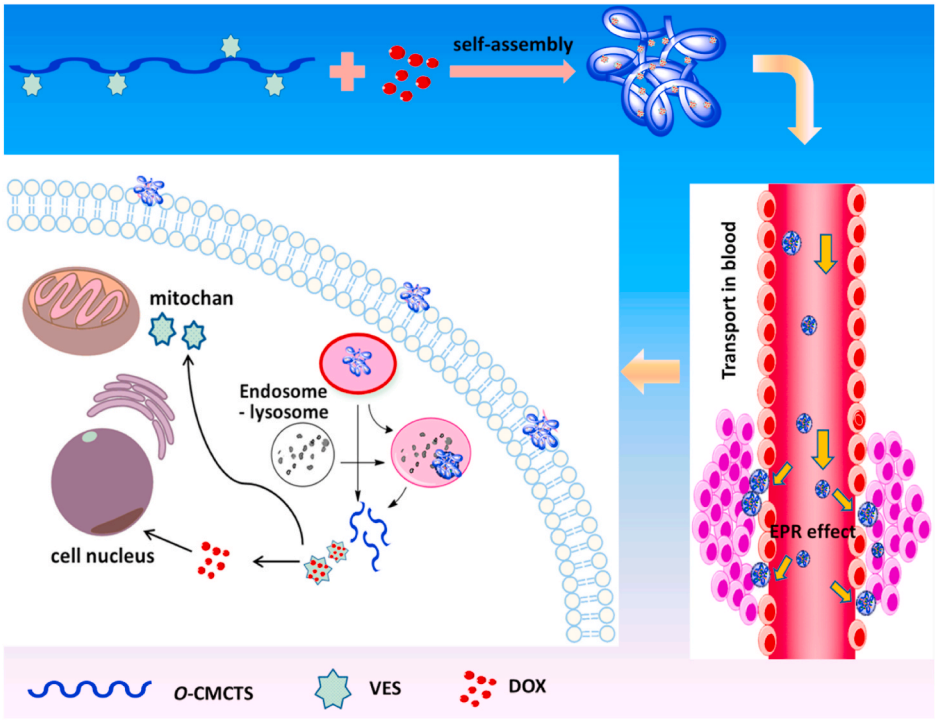

Scheme 1. Schematic diagram of the *O*-CMCTS-VES nanoparticles with EPR effect for anticancer therapy.

from Meilun Biotechnology Co. Ltd (Dalian, China). Dulvecco's modified Eagle's medium (DMEM) were purchased from Hyclone Inc. MTT (3-(4,5-dimethylthiazol-2-yl)-2,5-diphenyltetrazolium bromide) was purchased from Sigma-Aldrich (St. Louis, MO, USA). Fetal bovine serum (FBS) was purchased from Zhejiang Tianhang Biotechnology Co. Ltd (Zhejiang, China). All the solvents were obtained from Huasheng Reagent Co., Ltd. (Qingdao, China) and purified before used.

The human liver cancer cells HepG2, mouse fibroblast cells (L929) and mouse hepatoma 22 cells were supplied by Cell Bank of Chinese Academy of Sciences. Adult male Sprague-Dawley (SD) rats weighing 200 ± 20 g and Balb/C mice (half male and female) weighing 20±4 g were supplied by the Laboratory Animal Center of Shanxi Medical University in China, with certificate of SCXK (Jin) 20150001. All animals were kept under a 12 h light-dark cycles at consistent temperature (25 ± 3 °C) and relative humidity (60–70%). Experiments were performed in accordance with the ethical guidelines of the Shandong Province Experimental Animal Management Committee and were in complete compliance with the National Institutes of Health Guide for the Care and Use of Laboratory Animals.

2.2. Synthesis of the amphiphiles O-CMCTS-VES

The *O*-CMCTS-VES was synthesized as the following method. Briefly, the VES (1.59 g) was dissolved into 70 mL of DMF and then the EDC (2 eq. with VES) and NHS (2 eq. with VES) were added into the solution under stirring for 0.5 h at room temperature. Afterwards *O*-CMCTS with different weights (0.5 g, 0.66 g and 1.31 g) were dissolved into distilled water and added dropwise into the mixture solution, respectively. The solution was kept stirring at room temperature for 48 h. Then, the mixture solution was added to absolute ethyl alcohol (5 eq. volume with the mixture) to precipitate the solid product. The precipitate was washed with 100 mL absolute ethyl alcohol three times, and dissolved in distilled water. After that, the solution was dialyzed in distilled water using a dialysis membrane (MWCO 14 KDa, Spectra/Por, USA). The *O*-CMCTS-VES was obtained after freeze-drying. The chemical structure of the products was characterized by ^{1}H NMR (Agilent 500 MHz) and Fourier Transform Infrared Spectra (FTIS, Thermo Scientific Nicolet Nexus-470). And the substitution degree of VES in *O*-CMCTS-VES was determined by elemental analysis. According to the C/N, the degree of the substitution, which meant the number of VES groups per sugar ring of *O*-CMCTS-VES, was determined by TNBS method using a Euro Vector EA300 elemental analyzer. The degree of substitution was calculated by the following equation:

$$\text{Degree of substitution (DS)} = [m(C/N)_{CMCTS\text{-}VES} - m(C/N)_{CMCTS}]/n \times 100\% \quad (1)$$

Where $m(C/N)_{CMCTS\text{-}VES}$ was the mole ratio of carbon to nitrogen of CMCTS-VES, $m(C/N)_{CMCTS}$ was the mole ratio of carbon to nitrogen of CMCTS, and n was the number of moles of carbon in VES.

2.3. The method of labeling O-CMCTS-VES with FITC

100 mg of *O*-CMCTS-VES and 10 mg of FITC were dissolved into 100 mL of phosphate buffer solution (PBS, pH = 8) under stirring at 4 °C for 24 h. The mixture was dialyzed in 900 mL of distilled water in the dark using a cutoff tubing (MWCO 14 KDa, Spectra/Por, USA). FITC-*O*-CMCTS-VES was received after freeze drying and kept in the dark place.

Preparation and characterization of drug loaded micelles (DOX/*O*-CMCTS-VES).

O-CMCTS-VES and DOX·HCl (the weight ratio of *O*-CMCTS-VES to DOX·HCl was varied from 1:10 to 3:10) was dissolved in 10 mL distilled water. The triethylamine (2 eq. with DOX·HCl) was added into the mixture. After stirred at 4 °C for 24 h, the solution was centrifuged at 3000 rpm for 20 min and filtered with 1.2 μm filtration membrane [26]. The zeta potential and size of the micelles with or without DOX was evaluated by Dynamic Light Scattering (DLS, Malvern Zetasizer Nano ZS) and Scanning electron microscopy (SEM, Hitachi S4800).

The content of DOX was determined by ultraviolet–visible spectrophotometer at 485 nm in DMSO using calibration curve obtained from DOX/DMSO solutions with different DOX concentrations. Drug loading content (DLC) and encapsulation efficiency (EE) were calculated via the following formula:

$$DLC(\%) = \frac{\text{weight of the DOX in micelles}}{\text{weight of the micelles and the DOX}} \times 100\% \quad (2)$$

$$EE(\%) = \frac{\text{weight of the DOX in micelles}}{\text{weight of the toutal amount of the DOX}} \times 100\% \quad (3)$$

2.4. Molecular simulation of DOX/O-CMCTS-VES micelles

Molecular dynamics simulations of DOX/*O*-CMCTS-VES micelles were performed by using Materials Studio 6.0 software, Accelrys Inc. Forcite module was used to simulate the possible conformations and optimized the simulation under Compass field.

Energy minimization was carried out using the steepest descent minimization of 1000 steps followed by 9000 step conjugate gradient minimization at a constant pressure of 1 bar and a fixed temperature at 300 K. The step size was maintained at 1 fs.

2.5. Release profile of DOX/O-CMCTS-VES micelles

DOX/*O*-CMCTS-VES micelles were dispersed separately in pH = 5.7 and pH = 7.4 of PBS solution and then diluted to 1 mg/mL. The DOX/*O*-CMCTS-VES micelles solution (1 mL) was transferred to dialysis membrane tubes (MWCO 14 KDa, Spectra/Por, USA), which were immersed in flasks containing 25 mL of release medium. The flasks were put in a shaking bed at 37 °C under sink condition. 1 mL of solution was taken out as samples from the release medium and replaced with 1 mL of fresh PBS solution to keep the volume of solution constant. The released DOX was detected by a UV–vis spectrophotometer at 485 nm.

2.6. Cytotoxicity test

The cytotoxicity of blank *O*-CMCTS-VES micelles against L929 cells was evaluated by MTT assay. The L929 cells were planted in 96-well plates with the cell density of 8×10^3 cells per well with 200 μL medium for 24 h before treatment. The cells were then treated with *O*-CMCTS-VES micelles at given concentrations for another 24 h or 48 h. At the end of the treatment, the morphology of the cells was recorded by invert microscope (T1-SM100, Nicon, Japan). After that, 20 μL of MTT (0.5 mg/mL) were added in each well and the cells were further incubated for 4 h. The medium was removed and replaced with 150 μL of DMSO to dissolve the formazan crystals. The value of absorbance of the medium was tested at 492 nm by a microplate reader (Multiskan Go, Thermo Fisher Scientific, USA).

2.7. Blood compatibility evaluation

Further safety of *O*-CMCTS-VES micelles was tested by blood compatibility. 3 mL fresh blood were collected into blood collection tubes directly via SD rats and then diluted by 3 mL saline. 40 μL diluted blood was added respectively in containing different concentrations of *O*-CMCTS-VES micelles, in normal saline as negative control and in distilled water as positive control. After incubating for 1 h, the value of absorbance of supernatant was measured at 545 nm using a microplate reader (Multiskan Go, Thermo Fisher Scientific, USA). Hemolytic rate was calculated according to the following formulas:

$$\text{Hemolytic Rate}(\%) = (A_t - A_n)/(A_p — A_n) \times 100\% \quad (4)$$

Where A_t referred to the absorbance of the given concentrations

micelles, where A_n referred to the absorbance of negative control concentrations, where A_p referred to the absorbance of positive control concentrations.

2.8. In vivo preliminary safety evaluation

24 Balb/C male mice were randomly divided into two groups and were treated with 0.2 mL physiological saline (control group) and *O*-CMCTS-VES solution (experimental group) per day, according to the dose of 10 mg/kg (weight ratio of material weight to the body weight of the mice). On day 8, the blood of each mouse was extracted for coagulation capacity by using of four coagulation tests. The mice were sacrificed, and the samples of the heart, liver, spleen, lung, kidney and thymus were collected, weighted and routinely stained by HE method.

2.9. In vitro anticancer activity

HepG2 cells in logarithmic growth phase were harvested and seeded in 96-well plates at a density of 4×10^3 cells per well in 200 μL of RPMI 1640 medium for 24 h incubation before the tests. The culture medium was removed and replaced with 200 μl of medium containing DOX·HCl and DOX loaded micelles with the DOX concentrations ranging from 0.1 μg/mL to 100 μg/mL. After 24 h incubation, 20 μL of MTT solution were added in each well and the cells were incubated for 4 h at 37 °C with 5% CO_2. At the end of the treatment, the medium containing unreacted MTT was taken out and 150 μL of DMSO was added into each well to dissolve the formazan crystals. The value of absorbance was measured at 492 nm by a microplate reader (Multiskan Go, Thermo Fisher Scientific, USA).

2.10. Cellular uptake

HepG2 cells in logarithmic growth phase were seeded on 35 mm diameter glass dishes at a density of 2×10^4 cells per well. After incubating for 24 h, the culture medium was removed and the cells were incubated with the medium containing DOX·HCl and DOX loaded FITC-labeled nanoparticles (DOX concentration of 100 μg/mL) for 1 h, 3 h and 5 h. After that, the HepG2 cells were treated with Hoechst 33258 for 10 min and rinsed with PBS buffer for three times. The cells were observed under a confocal laser scanning microscope (CLSM, JM0L JSM-840). DOX was excited at 485 nm with emission at 595 nm. Hoechst 33258 was excited at 352 nm with emission at 461 nm. FITC was excited at 495 nm with emission at 525 nm.

2.11. In vivo antitumor activity study

H22 tumor-bearing Balb/C mice were obtained by injecting H22 cells (2×10^6 per mouse) into left flank subcutaneously and then randomly divided into three groups (Saline group, DOX·HCl group, DOX loaded *O*-CMCTS-VES micelles group) when the inoculated tumor volume came to 100–200 mm^3. Each group was injected via the tail vein at a dose of 5 mg DOX/kg at a 3 days interval, saline group was injected equivalent dose. After three times treatment, all mice were sacrificed at 9 d and then the heart, liver, lung, spleen, kidney as well as tumor were taken out, washed with saline, weighed and fixed in 4% formaldehyde for histological. The tumor inhibition radio was calculated using the following equation:

$$TIR\ (\%) = (1 - W_D/W_S) \times 100\% \quad (5)$$

where W_D referred to the tumor weight of the DOX·HCl or DOX loaded *O*-CMCTS-VES micelles groups, where W_S referred to the tumor weight of the saline groups, histopathological evaluation was explored by hematoxylin and eosin (H & E) stain assay.

2.12. Statistical analysis

All data were expressed as means ± SD of a representative of several similar experiments. Statistical difference between several groups was evaluated via a one-way analysis of variance (ANOVA), and a value of $P < 0.05$ was considered significant (computed by SPSS version 13.0 Software).

3. Results and discussion

The amphiphile of *O*-CMCTS-VES was synthesized as shown in Scheme 2. The detailed characterizations of the amphiphile of *O*-CMCTS-VES, including ^{1}H NMR, FT-IR and TNBS assay. The H^1 NMR spectra of the carboxymethyl chitosan *O*-CMCTS and the amphiphile of *O*-CMCTS-VES were shown in Fig. 1(A) and (B). It could be seen that the signals at 1.9 ppm was attributed to the proton of amino groups and hydroxyl groups were observed. The chemical shifts of the protons in sugar ring of *O*-CMCTS were concentrated from 3.2 to 4.4 ppm. The proton signals in *O*-carboxymethyl group were at about $\delta = 4.4$ ppm. The characteristic protons in methyl and methylene units of VES were observed at $\delta = 0.7$ ppm and $\delta = 1.1$ ppm, respectively [27]. The result indicated that VES was covalently grafted with free amino groups on carboxymethyl chitosan. Similarly, comparing the FT-IR spectra of *O*-CMCTS and *O*-CMCTS-VES (Fig. 1 (C)), the vibration absorption peak of *O*-CMCTS-VES at about 2930 cm^{-1} was sharper, indicating that the *O*-CMCTS molecule introduced a substituent group such as methyl or methylene. A strong absorption peak at 1607 cm^{-1} was observed, which was a characteristic peak of aromatic ring. Furthermore the appearance of the absorption band at 1383 cm^{-1} and 1248 cm^{-1} corresponding to $-CH_3$ stretching and C–O–C stretching of VES was observed, respectively. According to the infrared results, it could be judged that the VES had been covalently grafted to carboxymethyl chitosan. Moreover, the degree of the substitution of VES was calculated by TNBS assay [28] (Fig. 1 (D)). The results showed that the substitution degree of VES was 3.9% (CV-1), 3.7% (CV-2) and 2.4% (CV-3) at the different mol ratios (VES: *O*-CMCTS) of 0.75, 1 and 2, which promoted with the increasing amount of carboxymethyl chitosan. The reaction condition of CV-1 was the best comparing to CV-2 and CV-3. This was probably due to the reduction of the VES, and the amount of per glucosamine was increasing relatively. CV-1 was used in the following study.

The amphiphile of *O*-CMCTS-VES self-assembled into polymeric micelles in aqueous solution. To further evaluate the drug loading properties of the *O*-CMCTS-VES micelles, DLC and EE were used continually as considerable parameters. The drug loading contents were 6.1%, 13.0% and 10.6% with the weight ratio of DOX to *O*-CMCTS-VES corresponding 1:10, 2:10 and 3:10, and the corresponding EEs were 64.3%, 74.5% and 39.7% in Fig. 2 (A). The spatial capacity of the hydrophobic core of the polymeric micelles was limited when the weight ratio of DOX to *O*-CMCTS-VES came to 3:10. Excessive dosage resulted in greatly reduced filling efficiency of the hydrophobic core. Thus, the micelles prepared by the second drug loaded method were selected as the material for the subsequent experiment.

The size and zeta potential of the blank and drug loaded *O*-CMCTS-VES micelles were tested by DLS in Fig. 2(B) and (C). Both the two micelles were monodisperse in aqueous medium, and the mean sizes of blank and DOX-loaded nanoparticles were around 177 nm and 208 nm, respectively. The drug loaded nanoparticles exhibited bigger particle size comparing to the blank nanoparticles, which was probably caused by the enlargement of the hydrophobic core after drug loading. All the nanoparticles demonstrated a narrow size distribution (polydispersity index < 0.5). As for zeta potentials, both the two micelles were between −20 mV and −30 mV, which facilitated the long blood circulation. In addition, in Fig. 2(D) and (E), the blank and the drug-loaded nanoparticles were mostly spherical, nearly no agglomeration phenomenon was observed, and the particle size was distributed between 100 and 200 nm, which was consistent with the DLS results.

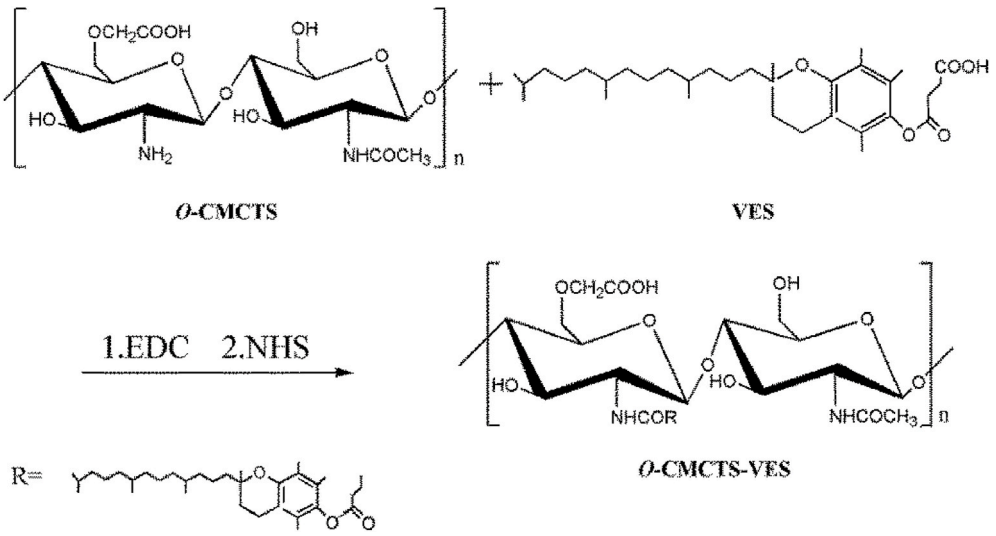

Scheme 2. Schematic diagram of the preparation of the amphiphilic self-assembled polymer.

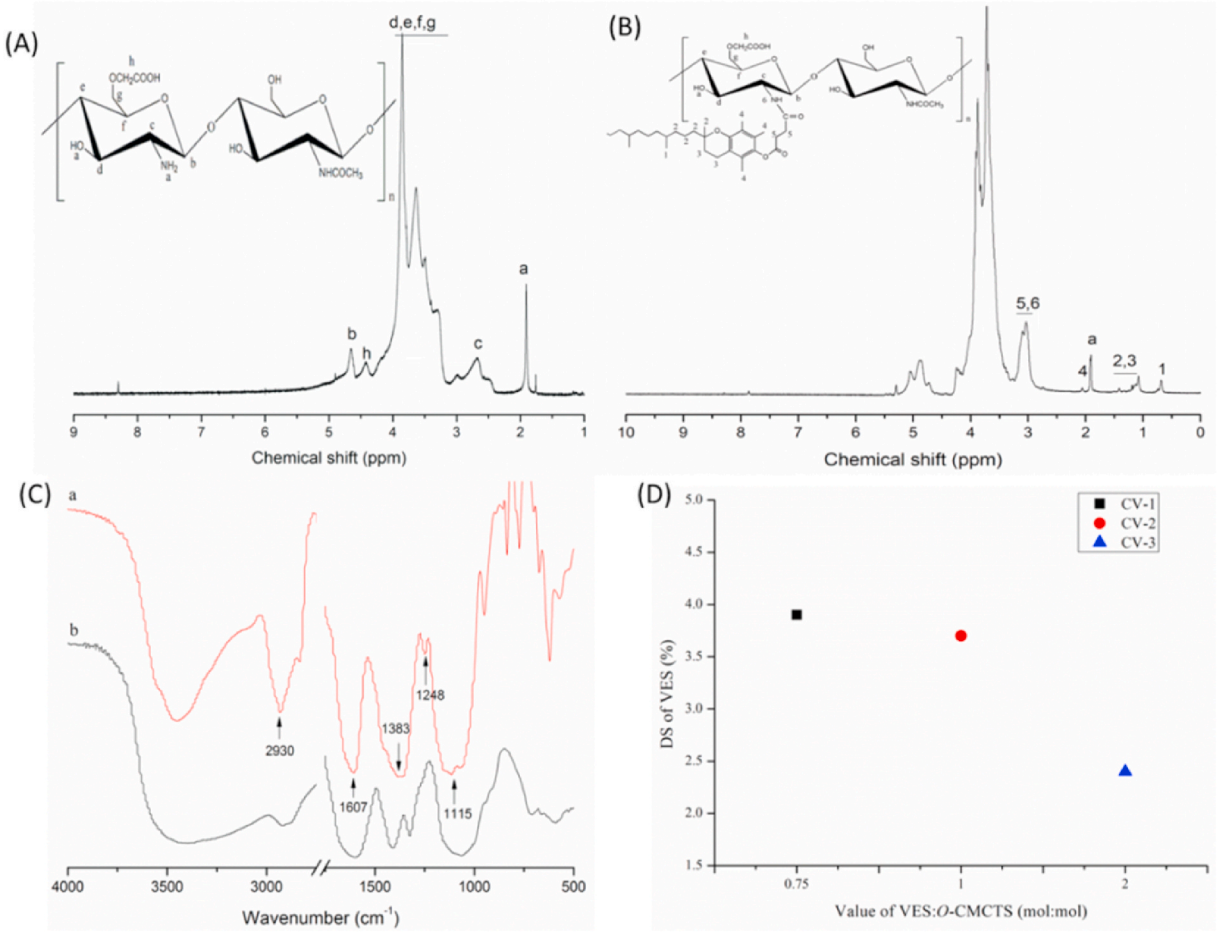

Fig. 1. The ^{1}H NMR spectra of *O*-CMCTS (A) and *O*-CMCTS-VES (B). The FTIR spectra of *O*-CMCTS-VES (C(a)) and *O*-CMCTS (C(b)). The substitution degree of VES in *O*-CMCTS-VES (D).

3.1. Molecular simulation

In order to find out the combination effect between the *O*-CMCTS-VES and the DOX, the molecular simulation test was operated. The result was showed in Fig. 3, three possible conformation types of DOX/*O*-CMCTS-VES were simulated, and the energies of the three different conformations were calculated, respectively. It was known that the lower the negative energy value was, the more stable structure it was. As the energy of type A was the lowest in the three conformations, it was the most stable form for DOX/*O*-CMCTS-VES molecule. The figure showed that DOX was tightly wrapped inside the molecule and spatially close to the functional groups of VES. The molecule of doxorubicin had a

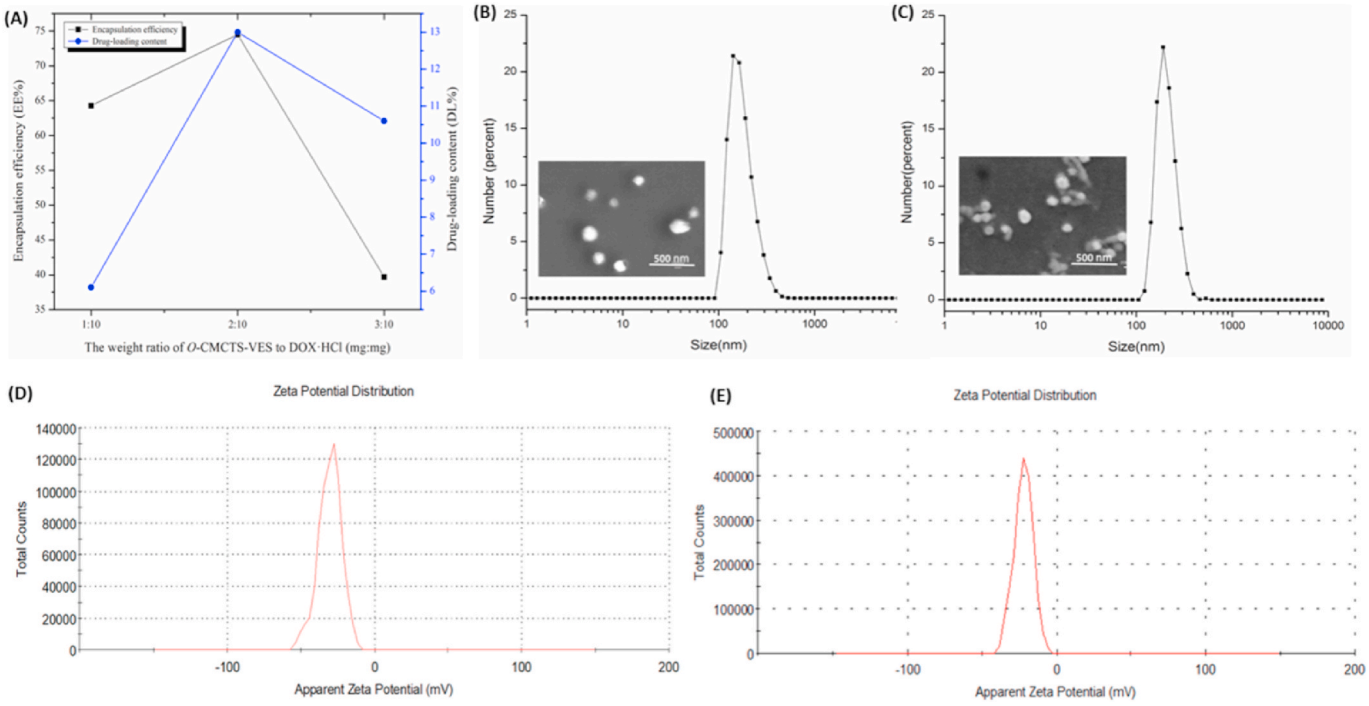

Fig. 2. The LC and EE with different mass ratios of DOX and *O*-CMCTS-VES (A). The size and SEM images of blank (B) and DOX-loaded micelles (C). The zeta potential of blank (D) and DOX-loaded micelles (E).

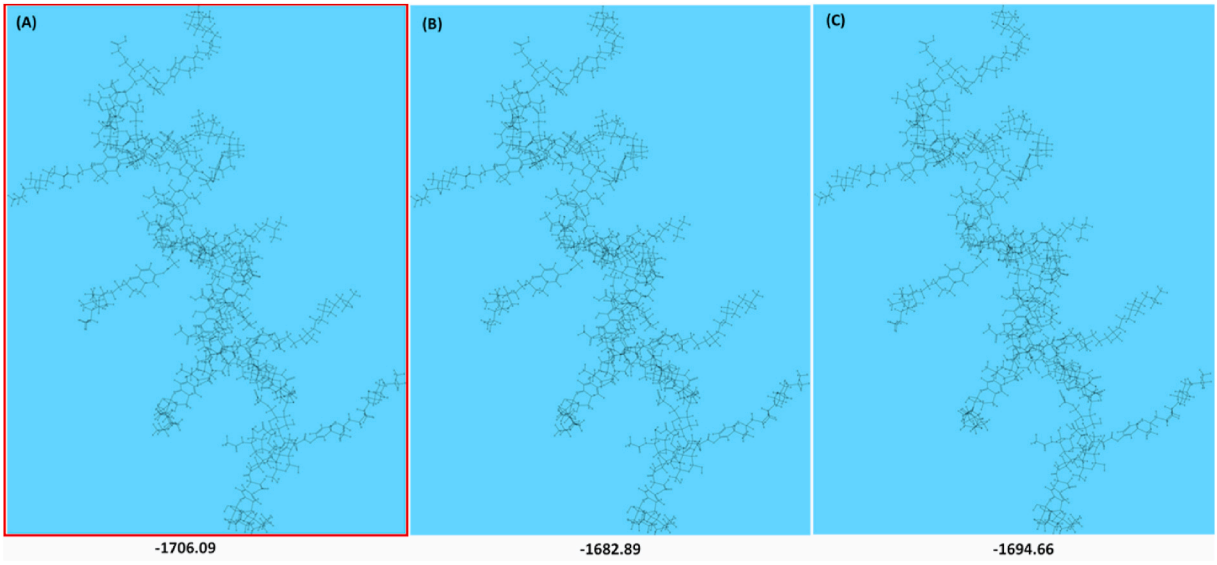

Fig. 3. The simulated conformations of DOX/*O*-CMCTS-VES molecule, the data were the calculated energy of the conformation (Unit: kcal/mol). (A) Type A, (B) Type B, (C) Type C.

typical anthraquinone structure and the structure of VES had a benzoxy-benzene ring. The rigid electron cloud planes were formed through the arrangement of the electron clouds, the DOX and the VES could produce a strong π-π conjugation effect. There were three forms of π-π interactions, the first was face to face, the second was offset and the third was edge to face. Calculated from the distance between the planes, the interaction between the DOX and the VES belonged to the first way. The results revealed the reason why the *O*-CMCTS-VES had a high drug loading content.

The *in vitro* drug release studies were performed in simulated tumor tissue environment (pH 5.7) and normal physiological environment (pH 7.4), respectively. The result in Fig. 4 (A) indicated that the release of DOX from DOX-loaded nanoparticles was pH-responsive. The release profile exhibited a burst release in the initial 4 h, about 58% and 45% in pH 5.7 and pH 7.4 conditions, relatively. And a followed sustaining release phase was observed both in simulated tumor tissue environment and normal physiological environment. In the first phase, the burst release was caused by escaping of DOX absorbed to the surface of micelles [29]. The followed sustaining release phase was due to the diffused DOX encapsulated in the hydrophobic cores. The DOX and the benzoxy-benzene ring in VES had strong conjugation effect, which could be the reason that led to the drug release rate at 88.7% in the end. After releasing 48 h, 58.2% of DOX was released from DOX-loaded nanoparticles in pH 7.4 PBS buffer whereas the drug release reached 88.7% in

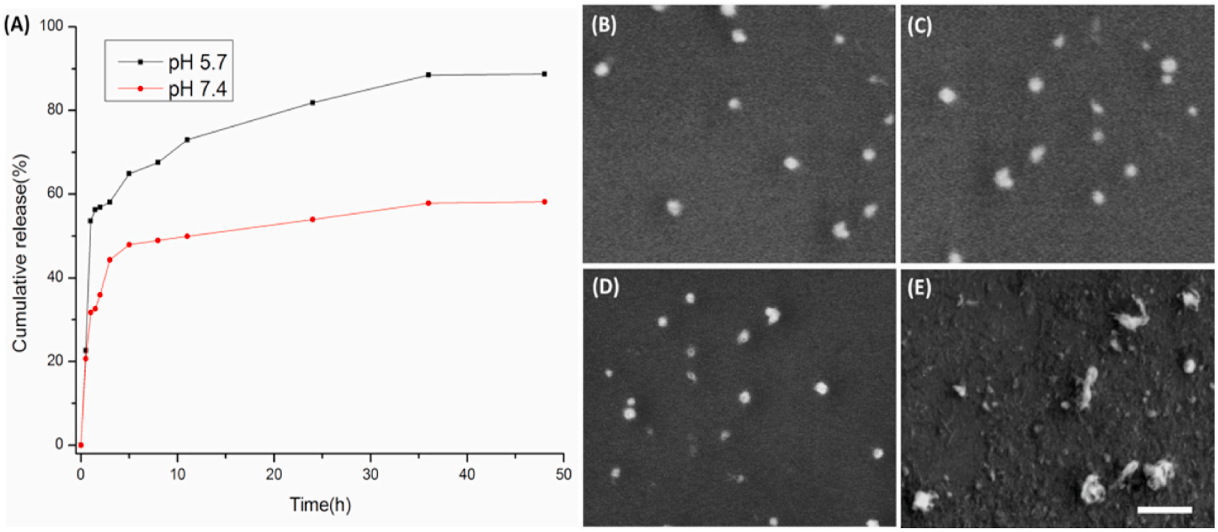

Fig. 4. (A) *In vitro* release of DOX/*O*-CMCTS-VES nanoparticles in PBS buffer solution with different pH values. (B) SEM image of *O*-CMCTS-VES nanoparticles at pH 7.4 for 0 h. (C) SEM image of *O*-CMCTS-VES nanoparticles at pH 7.4 for 24 h. (D) SEM image of *O*-CMCTS-VES nanoparticles at pH 5.7 for 0 h. (E) SEM image of *O*-CMCTS-VES nanoparticles at pH 5.7 for 24 h.

pH 5.7 PBS buffer. This was attributed to the protonation of amino groups of *O*-CMCTS-VES at acidic pH, which increased electrostatic repulsing among polymeric chains in the shell of micelles to lead to the increase of the drug release [30].

The SEM results were showed in Fig. 4 (B-E), which demonstrated that the diameters of the *O*-CMCTS-VES nanoparticles didn't change significantly after 24 h in the condition of pH7.4, and the nanoparticles still remained in regular circular shape. However, after maintained for 24 h under the condition of pH5.7, the diameters of the nanoparticles increased significantly from about 200 nm to more than 800 nm. Their shape were no longer regular circles, the structure dissolved and became into irregular shape. The results showed that the nanoparticles had typical pH sensitivity, their spherical structures could be destroyed rapidly in pH5.7 and their contents could be released effectively through such changes.

The cytotoxicity of blank *O*-CMCTS-VES nanoparticles was evaluated using the MTT assay. The nanoparticles were incubated with L929 cells with the concentrations ranged from 10 μg/mL to 500 μg/mL for 24 h and 48 h. The results were presented in Fig. 5 (A-C). The cell viabilities of all the groups were higher than 90% after 24 h incubation and were higher than 100% after 48 h incubation. It implied that the micelles had no cytotoxicity to L929 cells. The result of blood compatibility evaluation was shown in Fig. 5 (D). The results showed that when the material concentration was below 2 mg/mL, the hemolysis rate was less than 5% and the *O*-CMCTS-VES showed good blood compatibility. When the concentration of *O*-CMCTS-VES exceeded 2 mg/mL, the hemolysis rate

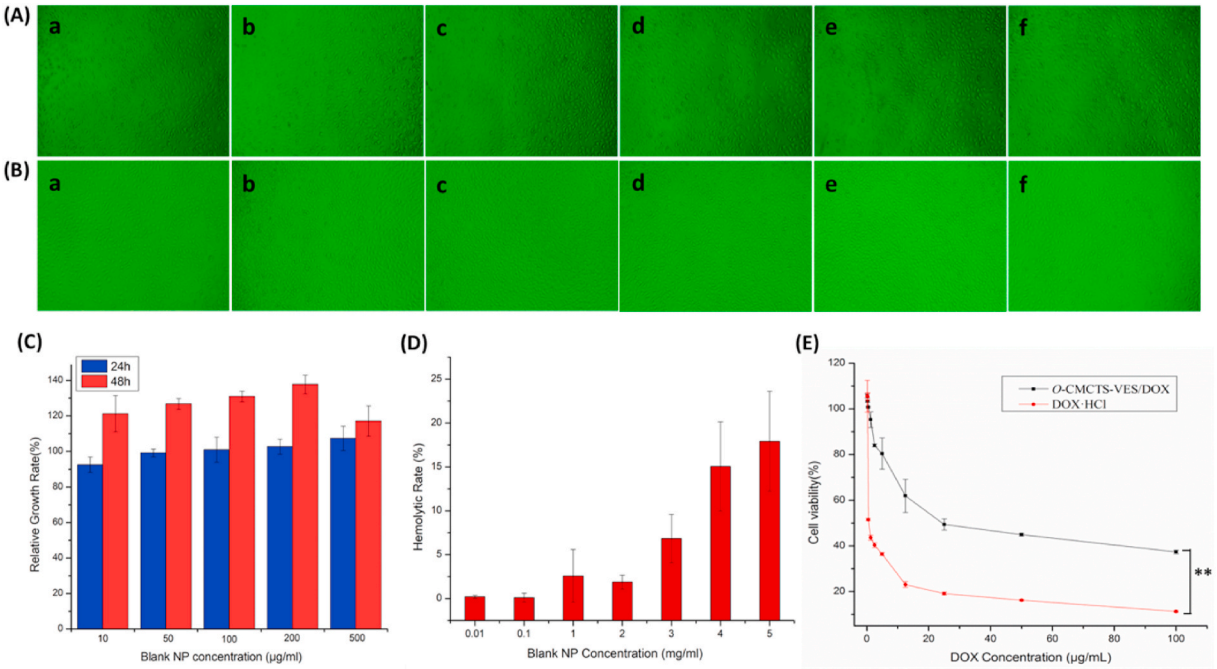

Fig. 5. Microscopic observation of L929 cells growth for 24 h (A) and 48 h (B): (a) 10 μg/mL, (b) 50 μg/mL, (c) 100 μg/mL, (d) 200 μg/mL, (e) 500 μg/mL, (f) control (40 ×). (C) The relative cell viability of the micelles incubated with L929 cells. (D) The hemolytic rate of the SD rats treated with different concentration micelles *in vitro*. (E) The *in vitro* anticancer activity of DOX/*O*-CMCTS-VES.

was greater than 5%. As we known, it was acknowledged that the material had bad hemocompatibility when the hemolytic rate was 5% above. It revealed that the material would be used at a concentration below 2 mg/mL in its further application.

The *in vitro* anticancer activity of DOX-loaded *O*-CMCTS-VES micelles was studied by MTT assay and the results were shown in Fig. 5 (E). The half maximal inhibitory concentration (IC_{50}) of free DOX·HCl and DOX/*O*-CMCTS-VES micelles to HepG2 liver cancer cells were 0.72 μg/mL and 24.08 μg/mL, respectively. The IC_{50} of DOX loaded micelles was higher than that of free DOX·HCl due to its diffusion internalization mode. The cellular uptake of free DOX·HCl was via passive diffusion and much faster than that of DOX-loaded NPs via endocytosis [31,32]. It was known that the passive diffusion was much faster than the endocytosis. The second reason was due to the controlled release effect of the *O*-CMCTS-VES micelles. The drug in the *O*-CMCTS-VES micelles was released gradually over time and it could not work as quickly as DOX·HCl. As a result, the IC50 of DOX loaded micelles was higher than that of free DOX·HCl. The *in vitro* tumor inhibiting rate for drug-loaded micelles could reach 62.57% with 24 h incubation.

For *in vivo* safety assessment, the PT, TT, AFTT and FIB values were measured on day 8 and the results showed that no significant difference between the two groups (Fig. 6 (A)). Furthermore, the tissue sections from the heart, liver, spleen, lung, kidney and thymus were weighted and assayed via HE staining method after intravenous administration. As shown in Fig. 6(B) and (C), compared with control group, no difference of visceral index was found and no indicators of damage were observed for these organs after treatment, suggesting that the *O*-CMCTS-VES did not cause systemic toxicity by intravenous injection.

The cellular uptake of the DOX-loaded FITC@*O*-CMCTS-VES micelles was investigated using CLSM. The results of HepG2 liver cancer cells treated with DOX-loaded FITC@*O*-CMCTS-VES micelles for 1, 3 and 5 h were shown in Fig. 7. The concentration of DOX was 100 μg/mL, and free DOX·HCl was used as control. It could be seen from the figure that the drug-loaded FITC@*O*-CMCTS-VES micelles significantly enhanced the cellular uptake comparing with the free DOX·HCl in 5 h. The strength of the red fluorescence in free DOX·HCl group was higher than that of drug-loaded *O*-CMCTS-VES group at 1 h and 3 h. This may be due to the fact that DOX·HCl enters the cell through passive diffusion [33]. So, the drug was taken up by cells rapidly in a short period of time. Whereas comparing with control group at 5 h, the higher red fluorescence intensity was observed in drug-loaded NPs group. It was attributed to that the cellular uptake of drug-loaded NPs was through endocytosis [34]. Moreover, both the cellular uptake of free DOX·HCl and drug loaded NPs were time-dependent.

The action mechanism of DOX was to embed the DNA bases to prevent the formation of mRNA, thus inhibiting the synthesis of DNA and RNA. It could be seen from Fig. 7 that the DOX mainly existed in the nuclear region. The dox concentrating presence in the nucleus region was more conducive to perform its function. The fluorescence of FITC was present in both the nucleus and cytoplasm, suggesting the distribution of *O*-CMCTS-VES in both the nucleus and cytoplasm. Dox fluorescence was weak and FITC fluorescence was strong in the cytoplasmic region, indicating that the *O*-CMCTS-VES and drug separated after entering the cell, and this behavior was speculated to mainly occur in the lysosome site. The FITC signal in the nucleus suggested that part of the *O*-CMCTS-VES might be degraded by enzymes such as lysozyme,

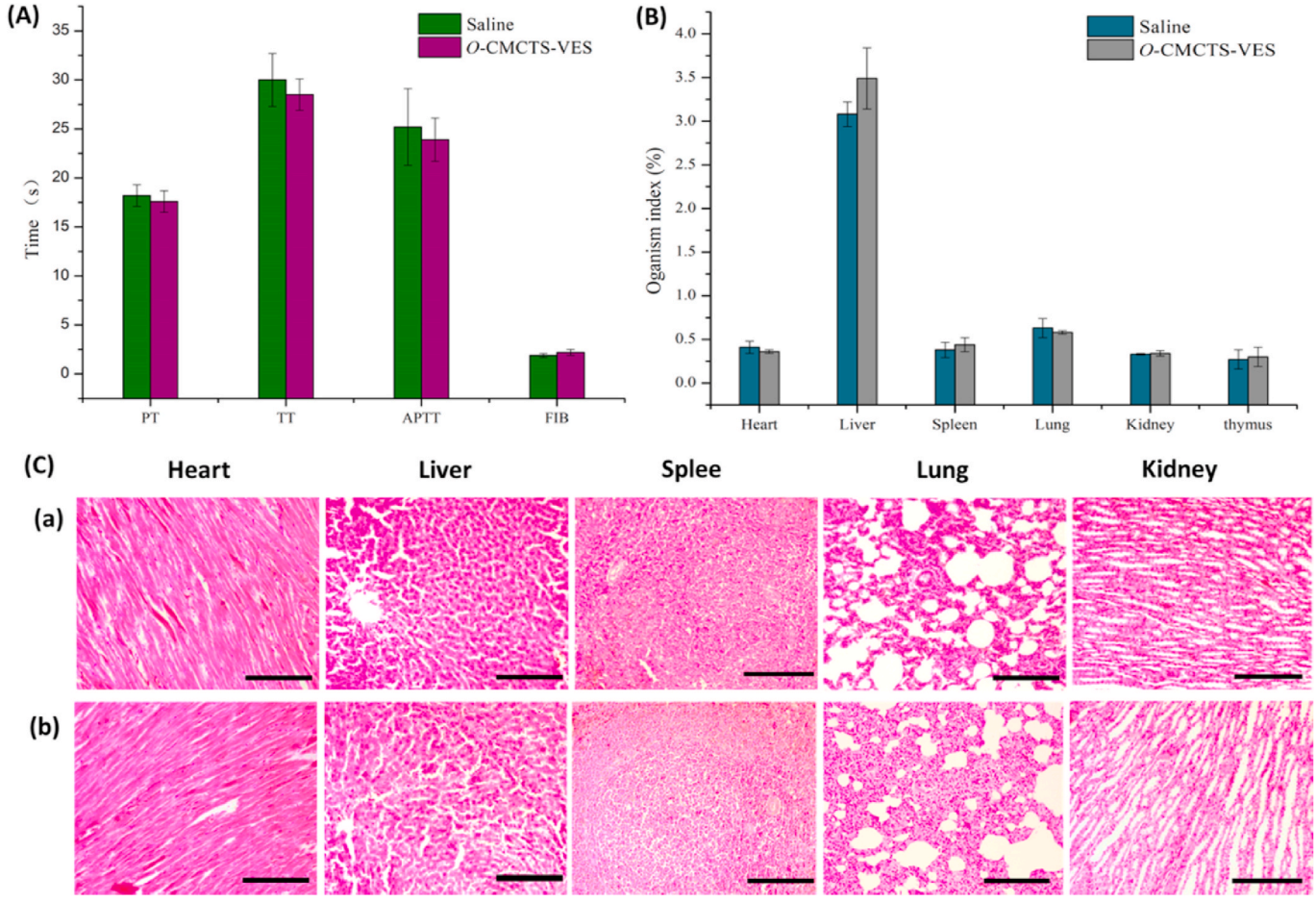

Fig. 6. In vivo safety evaluation of *O*-CMCTS-VES. (A) Coagulation ability of *O*-CMCTS-VES. (B) Calculation of mice viscera index by injection of *O*-CMCTS-VES. (C) HE staining of major organ sections (Bar = 20 μm). The data are presented as the means ± SD (n = 6). * indicates $P < 0.05$.

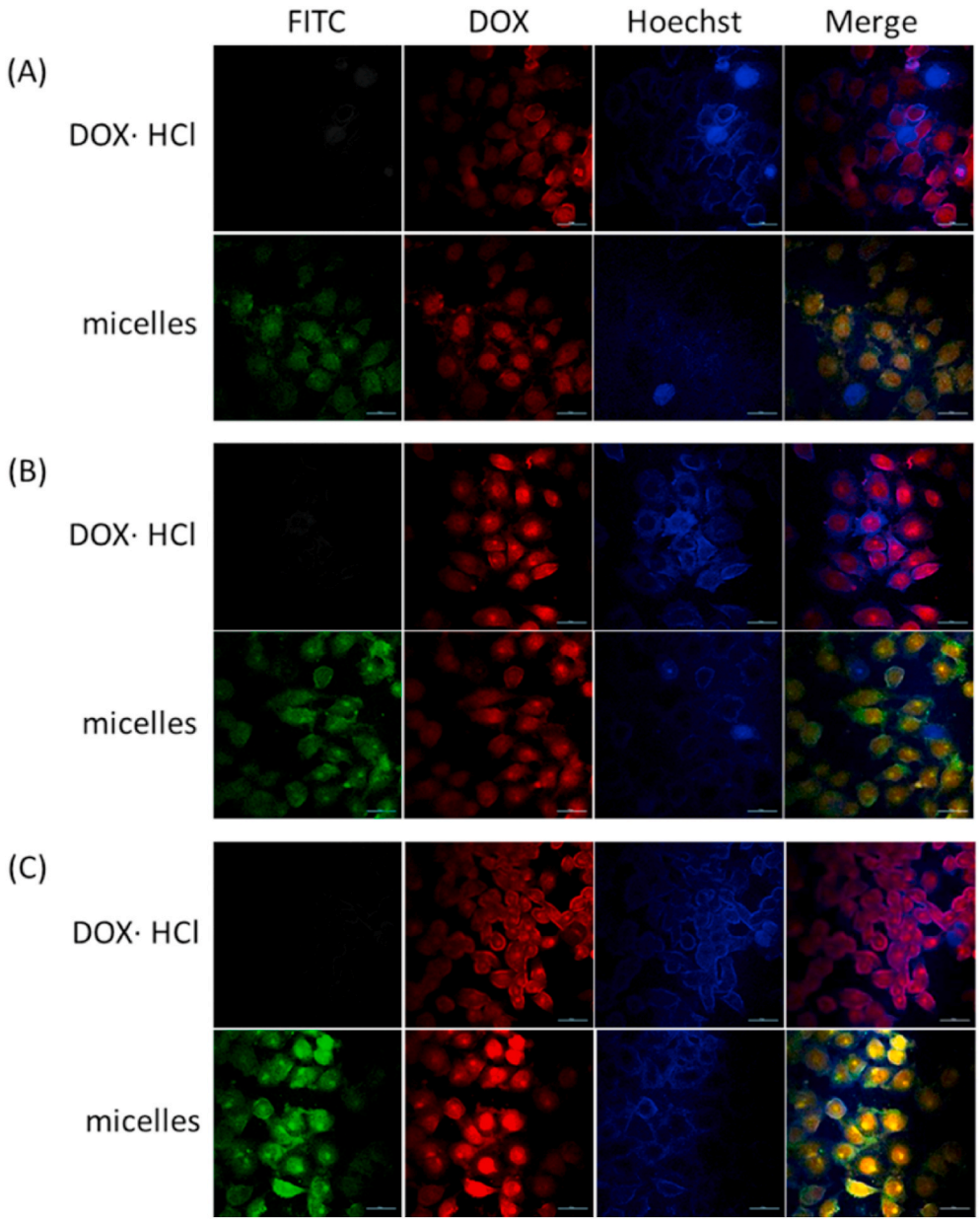

Fig. 7. Uptake of DOX· HCl and drug-loaded nanoparticles in HepG2 hepatoma cells for 1 h (A), 3 h (B) and 5 h (C) (Bar = 100 μm).

resulting in small molecular fragments, which were more conducive to its entry into the nucleus.

The *in vivo* antitumor effect of DOX/*O*-CMCTS-VES was demonstrated in Fig. 8. As shown in Fig. 8 (A), the weight of mice in the saline group increased significantly with the extension of time, while the mice both in DOX·HCl and DOX/*O*-CMCTS-VES groups lost weight under the influence of drugs. The mice in the DOX·HCl group lost their weight more obviously, which showed a significant difference from the control group at 9 days, indicating that the DOX· HCl had strong toxicity and had a great impact on the normal growth of mice.

The weight of tumor and the anti-tumor rate of all groups were shown in Fig. 8 (B). Both the free DOX·HCl and the drug-loaded micelles exhibited significantly tumor inhibition effect with a TIR of 48.04% and 35.58%, respectively. The histological tissues pictures of tumor, heart, liver, spleen, lung and kidney of the tumor-bearing mice were presented in Fig. 8 (C). The DOX·HCl group appeared liver toxicity for the observation of hepatic lobule. The gap between liver cells became larger and the tissue became looser, while the saline and drug-loaded NPs groups kept denser. It implied that the liver of mice injected DOX·HCl was impaired [35]. Distinctly disordered myofibrils (heart images in b, Fig. 8 (C)) and inflammatory cell infiltration accompanying by vacuolar degeneration of tissue (kidney images in Fig. 8 (C) b) were observed in DOX·HCl group [36]. There was no such side effect phenomenon in saline and drug-loaded NPs groups. The tumor tissue pictures of the DOX group and the drug-loaded material group exhibited the fact that the H22 cancer cells appeared different levels of apoptosis (tumor images in b and c, Fig. 8 (C)). In conclusion, the drug loaded micelles not only had perfect anti-tumor effect but also reduced the toxicity of DOX.

4. Conclusion

This study successfully designed amphiphilic self-assembled nanomicelles, which were prepared by the dehydration condensation of the carboxyl group of the carboxymethyl chitosan and the amino group of the vitamin E succinate. The micelles showed good stability and dispersion in aqueous media and nontoxic to L929 cells evaluated by *in*

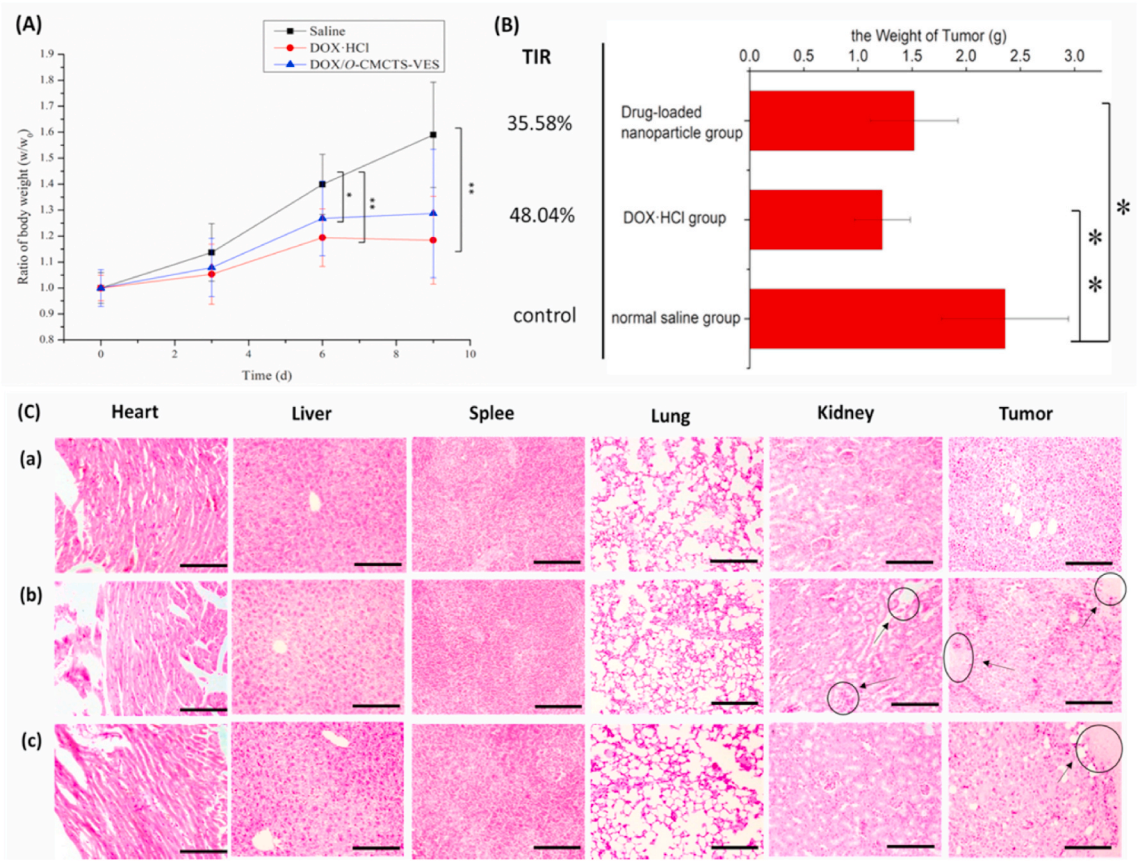

Fig. 8. *In vivo* antitumor effect of DOX/*O*-CMCTS-VES in 9 d. (A) Relative body weights of mice during cancer treatment. (B) The weight of tumor from mice treated with normal saline, DOX· HCl and DOX/*O*-CMCTS-VES NPs. And the antitumor rate of DOX· HCl and DOX/*O*-CMCTS-VES NPs. (mean ± SD, n = 10, $P < 0.05$ *, $P < 0.01$ **). (C) H & E stained sections of major organs from mice treated with normal saline (a), DOX·HCl (b) and *O*-CMCTS-VES/DOX NPs (c) (Bar = 20 μm).

vitro cytotoxicity. Hemolysis test and histocompatibility test showed that it had good biocompatibility *in vivo*. Drug-loaded nanoparticles were prepared with doxorubicin as a model drug for *in vitro* and *in vivo* anticancer experiments. *In vitro* drug release experiments implied good pH sensitivity and sustained-release effect. *In vitro* anti-tumor experiment showed that the drug-loaded nanoparticles could be efficiently taken up by HepG2 cancer cells and the tumor inhibition rate was up to 62.57%. *In vivo* anti-tumor experiments exhibited good tumor inhibition effect and could reduce the side effect of DOX apparently, and the drug-loaded micelles exhibited significantly tumor inhibition effect with a TIR of 35.58%. This amphiphilic nano-micelles was a promising carrier for drug delivery. The results suggested a promising carrier for drug delivery in the treatment of cancer and laid a good foundation for the application of CTS and VES.

CRediT authorship contribution statement

Xiaotong Chen: Investigation, Writing – original draft, Writing – review & editing. **Junxiang Gu:** Investigation, Writing – original draft. **Le Sun:** Formal analysis, Writing – review & editing. **Wenya Li:** Visualization. **Lili Guo:** Validation. **Zhiyang Gu:** Validation. **Litong Wang:** Visualization. **Yan Zhang:** Formal analysis. **Wangwang Zhang:** Formal analysis. **Baoqin Han:** Project administration. **Jing Chang:** Supervision, Conceptualization, Writing – review & editing.

Declaration of competing interest

The authors declare no conflict of interest.

Acknowledgement

The authors wish to thank National Natural Science Foundation of China (No. 51773188), Key Project of Natural Science Foundation of Shandong Province (No. ZR2020KE016), The National Key Research and Development Program of China (No. 2018YFC1105602, 2018YFD0900601).

Appendix A. Supplementary data

Supplementary data to this article can be found online at https://doi.org/10.1016/j.bioactmat.2021.02.028.

References

[1] C. Wang, Y. Li, S. Yan, H. Wang, X. Shao, M. Xiao, B. Yang, G. Qin, R. Kong, R. Chen, N. Zhang, Interactome analysis reveals that lncRNA HULC promotes aerobic glycolysis through LDHA and PKM2, Nat. Commun. 11 (2020), https://doi.org/10.1038/s41467-020-16966-3.

[2] K. Li, D. Li, L. Zhao, Y. Chang, Y. Zhang, Y. Cui, Z. Zhang, Calcium-mineralized polypeptide nanoparticle for intracellular drug delivery in osteosarcoma chemotherapy, Bioactive Materials 5 (2020) 721–731, https://doi.org/10.1016/j.bioactmat.2020.04.010.

[3] M.V. Liberti, J.W. Locasale, The Warburg effect: how does it benefit cancer cells? Trends Biochem. Sci. 41 (2016) 211–218, https://doi.org/10.1016/j.tibs.2015.12.001.

[4] Q. Qu, X. Ma, Y. Zhao, Anticancer effect of α-tocopheryl succinate delivered by mitochondria-targeted mesoporous silica nanoparticles, ACS Appl. Mater. Interfaces 8 (2016) 34261–34269, https://doi.org/10.1021/acsami.6b13974.

[5] S.E. Weinberg, N.S. Chandel, Targeting mitochondria metabolism for cancer therapy, Nat. Chem. Biol. 11 (2015) 9–15, https://doi.org/10.1038/nchembio.1712.

[6] J. Zhu, L. Zheng, S. Wen, Y. Tang, M. Shen, G. Zhang, X. Shi, Targeted cancer theranostics using alpha-tocopheryl succinate-conjugated multifunctional

dendrimer-entrapped gold nanoparticles, Biomaterials 35 (2014) 7635–7646, https://doi.org/10.1016/j.biomaterials.2014.05.046.
[7] Y.W. Won, S.M. Yoon, C.H. Sonn, K.M. Lee, Y.H. Kim, Nano self-assembly of recombinant human gelatin conjugated with α-tocopheryl succinate for Hsp90 inhibitor, 17-AAG, delivery, ACS Nano 5 (2011) 3839–3848, https://doi.org/10.1021/nn200173u.
[8] S. Martín-Saldaña, R. Palao-Suay, M.R. Aguilar, R. Ramírez-Camacho, J. San Román, Polymeric nanoparticles loaded with dexamethasone or α-tocopheryl succinate to prevent cisplatin-induced ototoxicity, Acta Biomater. 53 (2017) 199–210, https://doi.org/10.1016/j.actbio.2017.02.019.
[9] Y. Liu, Q. Li, X. Xiong, Y. Huang, Z. Zhou, Mitochondria-targeting and cell-penetrating peptides-co-modified HPMA copolymers for enhancing therapeutic efficacy of α-tocopheryl succinate, J. Mater. Chem. B. 6 (2018) 7674–7683, https://doi.org/10.1039/c8tb02621a.
[10] S.J. Ralph, S. Rodríguez-Enríquez, J. Neuzil, R. Moreno-Sánchez, Bioenergetic pathways in tumor mitochondria as targets for cancer therapy and the importance of the ROS-induced apoptotic trigger, Mol. Aspect. Med. 31 (2010) 29–59, https://doi.org/10.1016/j.mam.2009.12.006.
[11] R.G. Tuguntaev, S. Chen, A.S. Eltahan, A. Mozhi, S. Jin, J. Zhang, C. Li, P.C. Wang, X.J. Liang, P-gp Inhibition and Mitochondrial Impairment by Dual-Functional Nanostructure Based on Vitamin e Derivatives to Overcome Multidrug Resistance, ACS Appl. Mater. Interfaces 9 (2017) 16900–16912, https://doi.org/10.1021/acsami.7b03877.
[12] T.A. Debele, K.Y. Lee, N.Y. Hsu, Y.T. Chiang, L.Y. Yu, Y.A. Shen, C.L. Lo, A pH sensitive polymeric micelle for co-delivery of doxorubicin and α-TOS for colon cancer therapy, J. Mater. Chem. B. 5 (2017) 5870–5880, https://doi.org/10.1039/c7tb01031a.
[13] Z. Li, Q. Chen, Y. Qi, Z. Liu, T. Hao, X. Sun, M. Qiao, X. Ma, T. Xu, X. Zhao, C. Yang, D. Chen, Rational Design of Multifunctional Polymeric Nanoparticles Based on Poly (l -histidine) and d-α-Vitamin e Succinate for Reversing Tumor Multidrug Resistance, Biomacromolecules 19 (2018) 2595–2609, https://doi.org/10.1021/acs.biomac.8b00213.
[14] J.A.C.M. Goos, A. Cho, L.M. Carter, T.R. Dilling, M. Davydova, S. Puttick, A. Gupta, W.S. Price, J.F. Quinn, M.R. Whittaker, J.S. Lewis, T.P. Davis, Delivery of polymeric nanostars for molecular imaging and endoradiotherapy through the enhanced permeability and retention (EPR) effect, Theranostics 10 (2020), https://doi.org/10.7150/thno.36777.
[15] X. Sun, G. Wang, H. Zhang, S. Hu, X. Liu, J. Tang, Y. Shen, The blood clearance kinetics and pathway of polymeric micelles in cancer drug delivery. https://doi.org/10.1021/acsnano.8b02830, 2018.
[16] D. Hwang, J.D. Ramsey, A. V Kabanov, Polymeric micelles for the delivery of poorly soluble drugs: from nanoformulation to clinical approval, Adv. Drug Deliv. Rev. (2020), https://doi.org/10.1016/j.addr.2020.09.009.
[17] X. Zhang, N. Liang, X. Gong, Y. Kawashima, F. Cui, S. Sun, Tumor-targeting micelles based on folic acid and α-tocopherol succinate conjugated hyaluronic acid for paclitaxel delivery, Colloids Surf. B Biointerfaces 177 (2019) 11–18, https://doi.org/10.1016/j.colsurfb.2019.01.044.
[18] M. Gao, J. Deng, H. Chu, Y. Tang, Z. Wang, Y. Zhao, G. Li, Stereoselective stabilization of polymeric vitamin E conjugate micelles, Biomacromolecules 18 (2017) 4349–4356, https://doi.org/10.1021/acs.biomac.7b01409.
[19] H.B.T. Moran, J.L. Turley, M. Andersson, E.C. Lavelle, Biomaterials Immunomodulatory properties of chitosan polymers, Biomaterials 184 (2018) 1–9, https://doi.org/10.1016/j.biomaterials.2018.08.054.
[20] A. Anitha, V.V.D. Rani, R. Krishna, V. Sreeja, N. Selvamurugan, S.V. Nair, H. Tamura, R. Jayakumar, Synthesis , characterization , cytotoxicity and antibacterial studies of chitosan , O -carboxymethyl and N , O -carboxymethyl chitosan nanoparticles, Carbohydr. Polym. 78 (2009) 672–677, https://doi.org/10.1016/j.carbpol.2009.05.028.
[21] B. Li, J. Wang, Q. Gui, H. Yang, Bioactive Materials Drug-loaded chitosan fi lm prepared via facile solution casting and air-drying of plain water-based chitosan solution for ocular drug delivery, Bioact. Mater. 5 (2020) 577–583, https://doi.org/10.1016/j.bioactmat.2020.04.013.
[22] L. Upadhyaya, J. Singh, V. Agarwal, R. Prakash, The implications of recent advances in carboxymethyl chitosan based targeted drug delivery and tissue engineering applications, J. Contr. Release 186 (2014) 54–87, https://doi.org/10.1016/j.jconrel.2014.04.043.
[23] S.K. Jena, A.T. Sangamwar, Polymeric micelles of amphiphilic graft copolymer of α-tocopherol succinate- g -carboxymethyl chitosan for tamoxifen delivery : synthesis , characterization and in vivo pharmacokinetic study, Carbohydr. Polym. 151 (2016) 1162–1174, https://doi.org/10.1016/j.carbpol.2016.06.078.
[24] X. Wang, Y. Guo, L. Qiu, X. Wang, T. Li, L. Han, Preparation and evaluation of carboxymethyl chitosan-rhein polymeric micelles with synergistic antitumor effect for oral delivery of paclitaxel, Carbohydr. Polym. 206 (2019) 121–131, https://doi.org/10.1016/j.carbpol.2018.10.096.
[25] Y. Dai, S. Wang, W. Shi, M. Lang, pH-responsive carboxymethyl chitosan-derived micelles as apatinib carriers for effective anti-angiogenesis activity : preparation and in vitro evaluation, Carbohydr. Polym. 176 (2017) 107–116, https://doi.org/10.1016/j.carbpol.2017.08.011.
[26] H. Guo, D. Zhang, C. Li, L. Jia, G. Liu, L. Hao, D. Zheng, J. Shen, T. Li, Y. Guo, Q. Zhang, Self-assembled nanoparticles based on galactosylated O-carboxymethyl chitosan-graft-stearic acid conjugates for delivery of doxorubicin, Int. J. Pharm. 458 (2013) 31–38, https://doi.org/10.1016/j.ijpharm.2013.10.020.
[27] L. Catenacci, D. Mandracchia, M. Sorrenti, L. Colombo, M. Serra, G. Tripodo, In-solution structural considerations by 1 H NMR and solid-state thermal properties of inulin- D -α-tocopherol succinate (INVITE) micelles as drug delivery systems for hydrophobic drugs, Macromol. Chem. Phys. 215 (2014) 2084–2096, https://doi.org/10.1002/macp.201400342.
[28] H. Lian, J. Sun, Y.P. Yu, Y.H. Liu, W. Cao, Y.J. Wang, Y.H. Sun, S.L. Wang, Z.G. He, Supramolecular micellar nanoaggregates based on a novel chitosan/vitamin E succinate copolymer for paclitaxel selective delivery, Int. J. Nanomed. 6 (2011) 3323–3334, https://doi.org/10.2147/IJN.S26305.
[29] Y. Liang, X. Deng, L. Zhang, X. Peng, W. Gao, J. Cao, Z. Gu, B. He, Terminal modification of polymeric micelles with π-conjugated moieties for efficient anticancer drug delivery, Biomaterials 71 (2015) 1–10, https://doi.org/10.1016/j.biomaterials.2015.08.032.
[30] J. Liu, Y. Deng, D. Fu, Y. Yuan, Q. Li, L. Shi, G. Wang, Z. Wang, L. Wang, Bioactive Materials Sericin microparticles enveloped with metal-organic networks as a pulmonary targeting delivery system for intra-tracheally treating metastatic lung cancer, Bioact. Mater. 6 (2021) 273–284, https://doi.org/10.1016/j.bioactmat.2020.08.006.
[31] Y. Lei, Y. Lai, Y. Li, S. Li, G. Cheng, D. Li, H. Li, B. He, Z. Gu, Anticancer drug delivery of PEG based micelles with small lipophilic moieties, Int. J. Pharm. 453 (2013) 579–586, https://doi.org/10.1016/j.ijpharm.2013.06.001.
[32] Y. Pu, L. Zhang, H. Zheng, B. He, Z. Gu, Drug release of pH-sensitive poly(l-aspartate)-b-poly(ethylene glycol) micelles with POSS cores, Polym. Chem. 5 (2014) 463–470, https://doi.org/10.1039/c3py00965c.
[33] N. Li, N. Li, Q. Yi, K. Luo, C. Guo, D. Pan, Z. Gu, Amphiphilic peptide dendritic copolymer-doxorubicin nanoscale conjugate self-assembled to enzyme-responsive anti-cancer agent, Biomaterials 35 (2014) 9529–9545, https://doi.org/10.1016/j.biomaterials.2014.07.059.
[34] J. Chang, Y. Li, G. Wang, B. He, Z. Gu, Fabrication of novel coumarin derivative functionalized polypseudorotaxane micelles for drug delivery, Nanoscale 5 (2012) 813–820, https://doi.org/10.1039/c2nr32927a.
[35] Y. Lai, Y. Lei, X. Xu, Y. Li, B. He, Z. Gu, Polymeric micelles with π-π Conjugated cinnamic acid as lipophilic moieties for doxorubicin delivery, J. Mater. Chem. B. 1 (2013) 4289–4296, https://doi.org/10.1039/c3tb20392a.
[36] W. Gao, Y. Liang, X. Peng, Y. Hu, L. Zhang, H. Wu, B. He, In situ injection of phenylboronic acid based low molecular weight gels for efficient chemotherapy, Biomaterials 105 (2016) 1–11, https://doi.org/10.1016/j.biomaterials.2016.07.025.